4 Aerosol Deposition to Grassland

4.1 Introduction

GRAMINAE was a European Union funded project designed to study the GRassland AMmonia INteraction Across Europe. Ammonia is a naturally occurring trace gas, but concentrations are massively elevated (most significantly in source areas) by anthropogenic emissions, especially as a result of intensive agriculture. Ammonia has a variety of atmospheric and environmental effects, the most relevant of which are mentioned later in this chapter.

The aspect of the UMIST contribution to the project examined in detail in this chapter is the measurement of aerosol deposition fluxes during the integrated experiment held in Germany in May – June 2000. This chapter begins with an outline of the aims, methods and theory behind the integrated experiment, then, after a description of the aerosol flux measurement systems, explores the major results and concludes with a discussion of the implications of these. An analysis of the performance of the UMIST CPC flux measurement system is also included.

4.1.1 Aims of the Integrated Experiment

The GRAMINAE Integrated Experiment was conducted from the 21st May to the 15th June 2000 at an experimental managed grassland site at FAL (the Forschungs Anstalt für Landwirtschaft, – the German Federal Agricultural Research Institute in Braunschweig, 52^{o} 18’ N, 10^{o} 26’ W, 79 m amsl). Groups from throughout Europe involved in the GRAMINAE project attended, most contributing ammonia flux measurement systems. These were predominantly AMANDAs (ECN, Petten, the Netherlands; Wyers *et. al.*, 1993), used as profile concentration sensors for use with the gradient flux method (see chapter on micrometeorological methods). This aspect of the work was designed as an inter-comparison of the different systems being used in a North-West to South-East European transect for medium term monitoring.

The presence of a large number of ammonia gradient flux measurement systems on one site allowed unusually accurate measurements of ammonia fluxes to be made. To take full advantage of this and to assess the available experimental accuracy a number of further measurements were made as part of the integrated experiment. These included aerosol concentration, dynamics and composition, extensive plant physiological measurements and dew and leaf chemistry. UMIST contributed with the former two measurement types. It was hoped that, by use of these additional aerosol measurements, some insight could be gained into the interaction between ammonia and the aerosol phase over managed grassland. Specific questions of interest were quantification of the error induced in gradient flux calculations by non-conservation of ammonia fluxes near the surface (see next chapter on ammonia – aerosol interaction mechanisms), and the effect on the local aerosol population of grassland management practices.

A further opportunity afforded by this experiment , and the one investigated here, was the ability to measure aerosol deposition velocities to both long (≈ 0.75 m) and short (≈ 0.10 m) grass using the same measurement apparatus in the same location, as the grass canopy was cut during the campaign. This was the first time such an experiment on aerosol deposition had been conducted.

The following sections review the aerosol measurements made by UMIST as part of the integrated experiment, and the measurement site. Aerosol measurements made by other groups included ionic composition by Steam Jet Aerosol Collector (SJAC; ECN, Netherlands) and coarse mode concentrations using an Aerodynamic Particle Sizer (TSI 3320 APS; CEH Edinburgh, UK). However, these results are not used heavily here, and will be introduced only as necessary.

4.1.2 The Site

The field site for the integrated experiment was part of the FAL. An experimental field with considerable infrastructure and backup measurements was made available (Sutton *et. al.*, 2002). Ammonia concentration and flux measurements were made at several points in the field, but all aerosol measurements were concentrated in the

centre. Figure 1 shows a schematic representation of the distribution of experimental equipment.

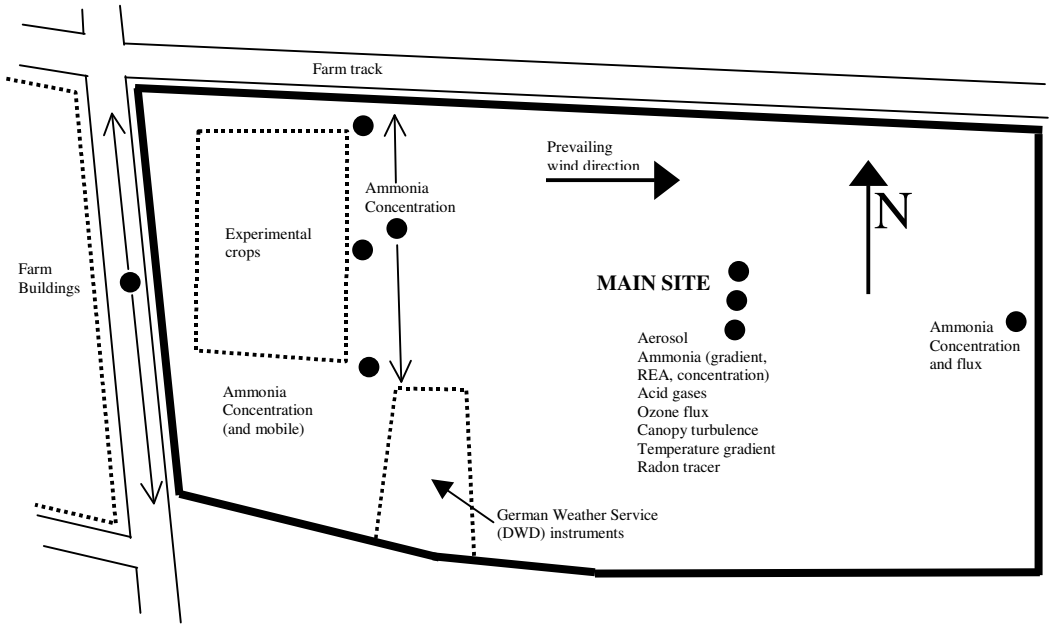

Figure 1. Schematic map of GRAMINAE field site. The symbols (•) represent ammonia concentration or flux measurements. Arrows (→) show the range and direction of mobile measurements.

All UMIST instruments were deployed on the main site, as indicated in figure 1. These are described in detail in the following section, but included the CPC flux system, two accumulation mode aerosol flux systems (ASASP-X / Gill 1012 R) and a Differential Mobility Particle Sizer (DMPS).

The length of the managed grassland fetch from the main site in the prevailing wind direction (Figure 1) was greater than 500 m.

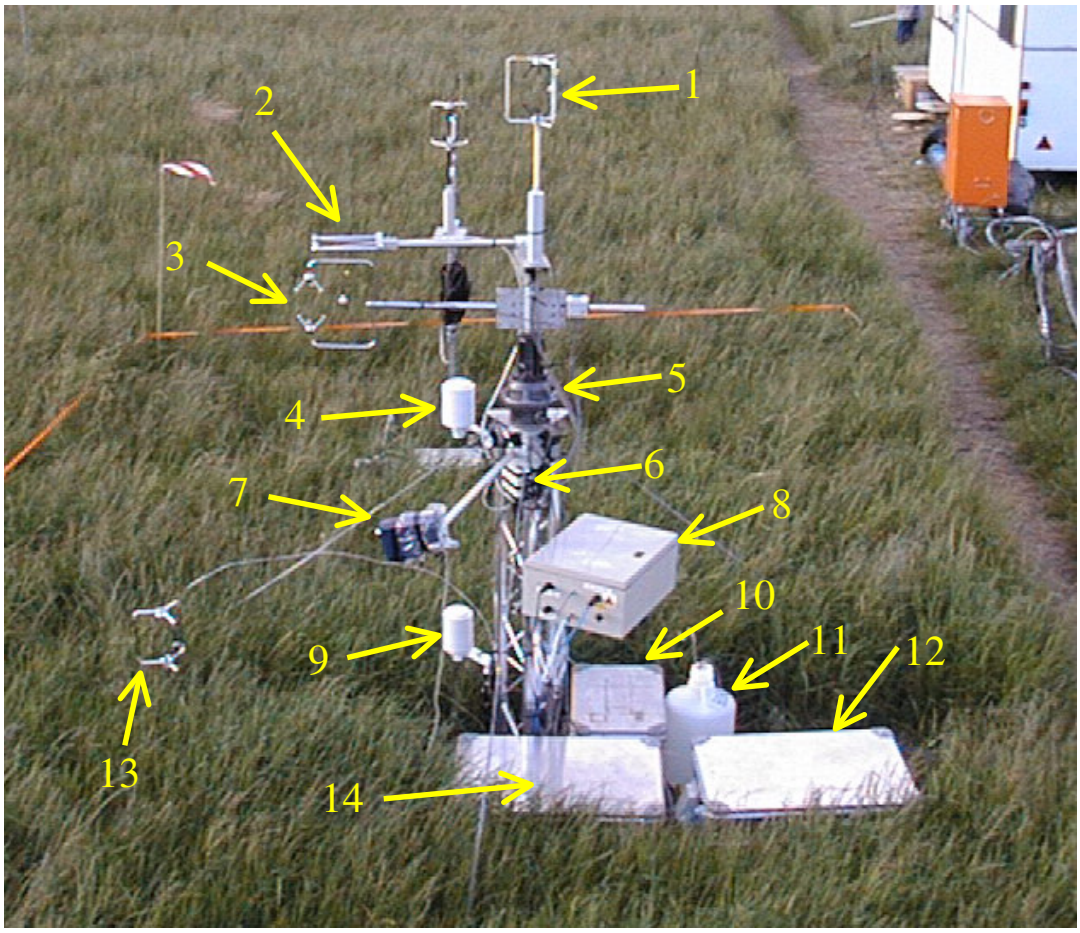

Figure 2. UMIST micrometeorology mast. The fourth anemometer visible in the background is part of a separate flux measurement system (CEH). The mobile lab housing the DMPS and the logging computers is visible in the top right of the picture.

The labels indicate:

1	–	Top Gill 1012 R
2	–	Campbell KH2O (fast water vapour)
3	–	Gill HS anemometer
4	–	Vaisala Humicap / PRT (CPC system)
5	–	Rotator
6	–	Vaisala PT 100 B (pressure)
7	–	IR Pyranometer (surface temperature)
8	–	CPC (in waterproof enclosure)
9	–	Vaisala Humicap (top ASASP-X system)
10	–	Power distribution and CPC pump
11	–	Butanol trap for CPC exhaust
12	–	ASASP-X (top flux measurement)
13	–	Lower Gill 1012 R
14	–	ASASP-X (lower flux measurement)

4.1.3 Measurements

The micrometeorological measurements discussed in this chapter were taken from a single small mast, the height of which was designed as a compromise between keeping the measurement footprint within the field and measuring at a large enough height that unreasonable frequency response requirements were not placed on the aerosol sensors (see later section on CPC system performance). Figure 2 shows a view of this mast.

Instrument	Height (m)
[1]Gill 1012 R Anemometer # 1	2.86
[1]ASASP-X # 1 (counter)	2.86
[1]Humicap (T and RH)	0.72
[1]KT19 IR Pyranometer	1.58
[2]Gill HS Anemometer	2.02
[2]KH2O UV Hygrometer	2.27
[2]CPC (counter)	2.02
[2]Humicap (T and RH)	1.68
[2]PT100B Pressure Transducer	1.41
[3]Gill 1012 R Anemometer # 2	0.70
[3]ASASP-X # 2 (counter)	0.70
[4]DMPS Inlet (17 m North)	~2.3

Table 1. Measurement heights for main equipment. Superscripts indicate which instruments formed parts of individual systems (*i.e.* [1], [2], [3] denote the higher ASASP-X system, the CPC flux system and the lower ASASP-X system respectively).

The accumulation mode aerosol fluxes measured using the two Gill 1012 R and ASASP-X combination systems are not discussed in great detail here, although the micrometeorological data were used by the project organisers to derive the "site average" parameters for use in the final ammonia gradient flux calculations (Hargreaves *et. al.*, 2002; Milford *et. al.*, 2002). The accumulation mode aerosol fluxes are, however, presented as estimates of deposition velocity to a variable height canopy. Data from the KT19 infra-red pyranometer were also used in estimates of

stomatal conductance by other groups (Hermann *et. al.*, 2002), but this does not form part of the current work.

The operation of the CPC flux system is outlined in a separate chapter. The ASASP-X based accumulation mode flux measurement systems work along similar lines, with fluxes being calculated by the Eddy Covariance method. The only substantial differences between the ASASP-X and CPC systems are that the ASASP-X resolves particle diameter between 0.1 μm < D_p < 3 μm, and in the technical aspects of the logging and analysis software. The differences are not sufficiently important for the current work to go into detail (see Gallagher *et. al.*, 1997 (b) for a general description of the system).

Table 1 gives details of the exact heights of the instruments shown in figure 2. The DMPS inlet was located some 17 m to the North (figure 1) of this mast, still on the main site, at a height of 2.3 m (given in table 1).

4.1.4 Management Practices

22nd May	Start of measurements (1200 GMT)
29th May	Grass cut (am, CEST)
30th May	Grass turned (am / pm, CEST)
31st May	Grass lifted (noon, CEST)
5th June	Field fertilised (am, CEST)
15th June	End of measurements (1200 GMT)

Table 2. Timing of management events during the GRAMINAE integrated experiment. Times are approximate due to the long duration of each "event" (~ ½ day).

As stated, a major project goal was to gain some insight into the effects of common grassland management practices on ammonia and aerosol fluxes and concentrations. Measurements were made continuously from the 22nd May at 1200 GMT (1400 CET,

local time) to the 15th June at 1200 GMT. Table 2 shows the timing of the management events for reference later in this chapter and the next.

4.2 Accumulation Mode Results

The results from the GRAMINAE integrated experiment in terms of aerosol dynamics can be conveniently subdivided into three distinct periods. During the first of these (for brevity referred to as the long canopy period), aerosol deposition to a long grass canopy (canopy height, h_c = 0.65 m to 1.00 m, mean around 0.75 m) was measured. This period lasted from the 22nd to the 29th May, – from the start of the experiment to grass cutting. The period from the 29th to the 31st May, when cut grass was drying in the field has been left out of this analysis due to the short duration of the period and the difficulty in interpreting results over such a complex surface.

The second period of interest was that from the 31st of May to the 5th of June, after the cut grass had been lifted (referred to as the short canopy period). Here aerosol deposition to a short grass canopy (h_c = 0.07 to 0.14 m, mean 0.10 m) was observed. This allowed the contrast between deposition to a long and short canopy using static measurement equipment to be examined.

The final period to be investigated in depth ran from the 5th to the 15th of June. The field was fertilised with 100 kg N ha^{-1} as Calcium Ammonium Nitrate in pellets on the 5th of June. During this period (the post-fertilisation period), the effects of ammonia emission on the aerosol population could be observed. Results from this period of measurements are reserved until the next chapter on ammonia – aerosol interactions.

4.2.1 Surface deposition velocity

Using equations 2.33, 2.34 and 2.36, it is simple, assuming only two components of resistance to deposition (aerodynamic and surface), to calculate the surface deposition velocity. All deposition velocities presented here are *surface* deposition values (*i.e.* with the aerodynamic resistance component removed). This is common practice in the

literature, and allows direct comparison of different canopy types (morphology, stomatal activity *etc.*) without reference to meteorological conditions.

4.2.2 Deposition Velocity Above a Managed Grass Canopy

Measurements of aerosol deposition to various surfaces have been conducted by a number of researchers over the last twenty years, since Weseley (1977) and Sievering (1981) first outlined the application of the eddy covariance technique to aerosol flux calculation. Generally, in these studies, optical scattering devices have been used to count particles and size them according to Mie theory (the relationship between scattered light intensity and particle diameter, D_p). For completeness the Eddy Covariance equation for these size-segregating instruments is presented here.

$$f_\chi(D_p) = \overline{w'\chi'(D_p)} \qquad (4.1)$$

This is identical to the equation presented in chapter two (2.22) except that $f_\chi(D_p)$ is the size resolved flux, and $\chi'(D_p)$ is the Reynolds decomposed fluctuating component of aerosol concentration in the size range indicated by D_p.

Optical scattering instruments give important data on the particle diameter dependence of aerosol fluxes, and can be used to infer mass fluxes. However, they suffer severely from the counting statistical problems outlined in chapter two (equations 2.26 – 2.28). The instruments typically operate at low flow rates (2 cm^{-3} s^{-1} for the ASASP-X probes used in this study). This gives rise to very low numbers of aerosol being counted producing a large standard error and a consequently large uncertainty in the calculated flux. The effect of the low flow rate is compounded by the speciation of concentration by aerosol diameter. When fluxes are calculated for narrow ranges of D_p, the total number of aerosol counted in the size range can be extremely low, and it was found that at the ambient concentrations encountered in this project, reliable fluxes of aerosol larger than around 1 μm could not be calculated without very heavy time averaging. The average total number concentration of particles in the size range 0.1 μm < D_p < 3 μm detected by the upper ASASP-X

system throughout the campaign was 290 cm^{-3} compared to 7916 cm^{-3} in the range 0.011 μm < D_p < 3 μm by the CPC flux system.

Nevertheless, size resolved aerosol deposition velocities over both canopy heights have been calculated, and fit very well with other published values when the surface roughness length is taken into account. Figure 3 shows the deposition velocities calculated from the top ASASP-X / Gill 1012 R system. These are the fluxes of particles of diameter 0.1 μm < D_p < 0.2 μm, averaged over the first and second periods (long and short canopies respectively, before fertilisation) under conditions of near neutral stability. The values were obtained as the average of all deposition events (calculated over a 15 minute averaging period). The figure is modified from Gallagher *et. al.* (2002). Roughness lengths are averages of all values calculated with 15 minute averaging periods over the same periods as the aerosol deposition velocities. Figure 3 also contains deposition velocities calculated by other authors over different surfaces, and shows a strong, systematic dependence on roughness length.

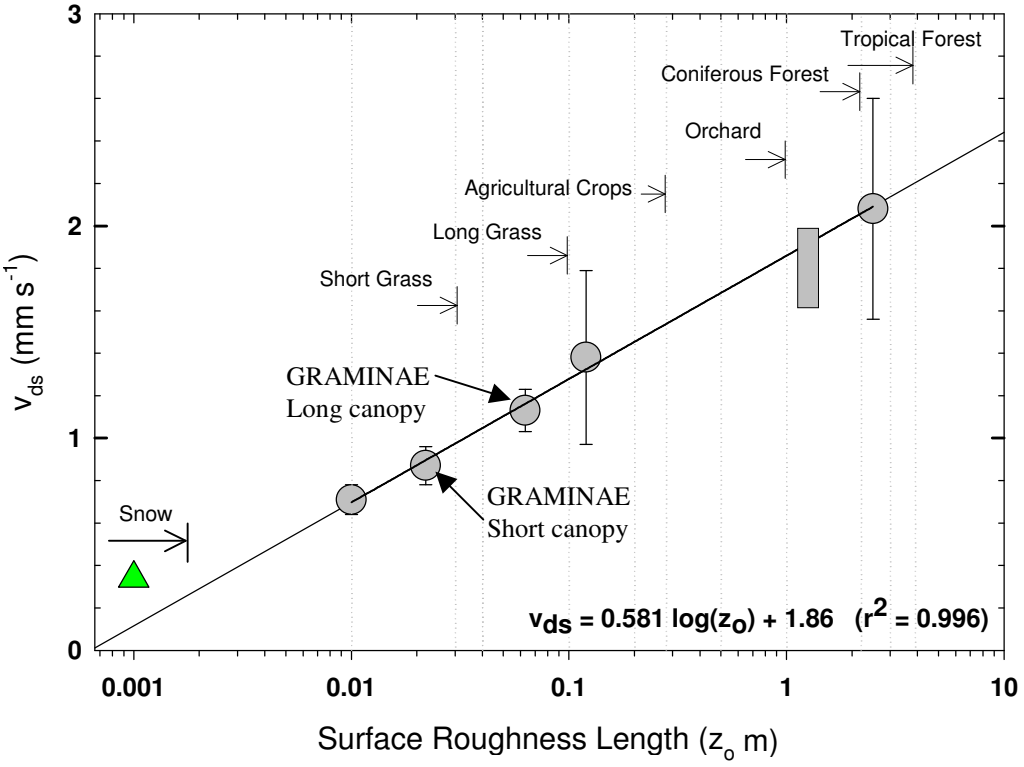

Figure 3. Aerosol (0.1 μm < D_p < 0.2 μm) deposition velocities as a function of roughness length, values taken during near neurtal conditions in order to remove any confounding by stability dependence. GRAMINAE results are highlighted.

For the long canopy (shown in figure 3), the mean deposition velocity (z_0 = 0.063 m) was 1.13 mm s^{-1}. After the canopy was cut (z_0 = 0.022 m), the mean deposition velocity fell to 0.87 mm s^{-1}. The main relevant canopy parameters and the deposition velocities are shown in table 3.

	Mean v_{ds} (mm s^{-1})	Mean χ (cm^{-3})	σ_{vds} (mm s^{-1})	σ_{χ} (cm^{-3})	z_0 (m)	h_c (m)
Long canopy	1.13	240.8	0.10	23.95	0.063	0.65 – 1.00
Short canopy	0.87	321.4	0.09	21.81	0.022	0.07 – 0.14

Table 3. Summary of accumulation mode (0.1 μm < D_p < 0.2 μm) aerosol deposition data. v_{ds} = surface deposition velocity, χ = concentration, z_0 = roughness length, h_c = canopy height, σ = standard deviation (presented as a measure of the variability of the calculated quantity).

For the reasons given above, individual values of aerosol fluxes from the ASASP-X systems were uncertain, and the time series of size segregated flux were consequently very noisy. The variability of the results also precludes the use of this data in the calculation of ammonia uptake rates to aerosol. Accumulation mode aerosol deposition fluxes will therefore not be pursued further. The following section is devoted to an investigation of the performance of the CPC flux measurement system, with a view to assessing the reliability of the measured fine mode aerosol fluxes.

4.3 Performance of the CPC flux system

The ASASP-X / Gill 1012 R accumulation mode aerosol flux measurement systems referred to above were logged at 20.86 Hz. The system response at high frequency should have been limited only by damping of concentration fluctuations (particle losses) in the inlet tube. Since the size range considered here is too large to suffer large diffusional losses to the tube walls, and too small to impact efficiently on bends in the tube, it is assumed that the inlet damping was not significant. This means that the measured fluxes should be accurate.

Aerosol fluxes in the size range 0.011 μm < D_p < 3 μm measured by the CPC system may, however, have been affected by "damping" as explained in chapter 3. Measurement of aerosol fluxes using CPC instruments is a recent development, and there are potential problems related to instrument response time. In the more commonly used ASASP-X type optical scattering instruments, aerosol are detected instantly on entering the optical scattering chamber. In CPC type instruments, aerosol must first be "grown" in an environment saturated with Butan-1-ol vapour. This gives rise to doubts over the response time of the instrument, and whether there is increased scope for particle losses and damping of the aerosol concentration time series, causing fluxes to be under-estimated.

The only way to resolve these questions and to confirm the validity of the flux results from the CPC system is to examine the power spectra and co-spectra of the *w'* and *N'* time series (chapter 2). These are referred to as the *W* and *N* power spectra in the following, for simplicity, – note that the actual time series analysed are the Reynolds decomposed perturbation parts. The issue did not arise in the analysis of the SASUA data (chapter 6) because of the long time scale of the turbulence contributing to aerosol transport at the large measurement height used in that experiment. During GRAMINAE, however, the anemometer and aerosol inlet were located at z_m = 2.02 m. As explained in chapter 2 (equation 2.4), this reduces the time scale on which the aerosol transporting turbulence is expected to operate.

4.3.1 Power spectral analyses

The first analysis to be conducted is an examination of the power spectra of *W* and *N*. These will confirm that the vertical wind speed and concentration follow the familiar spectral predictions (*e.g.* Kolmogorov 1941, Kaimal *et. al.* 1972) and hence have been correctly measured. Examination of the *N* power spectrum should also show the frequency response of the CPC and specifically, the maximum resolvable frequency of aerosol concentration fluctuations.

It is common practice in the literature to denote the frequency on the abscissa in non-dimensionalised form, as $f = n_r\, z/U$, where n_r is the radial frequency in rad s^{-1}, z is

measurement height and U is wind speed. This is intended to account for the effects of wind speed and measurement height for different experimental arrangements; – the normalisation should cause the inertial sub-ranges of different spectra to collapse to a common curve and allow for ease of comparison. However, as the purpose of this section is to examine the characteristics of the CPC flux measurement system and not the turbulence structure observed, it is most appropriate to use the natural frequency (in Hz) as the ordinate in the following. Plots shown in this section are also natural frequency weighted.

4.3.2 Vertical wind speed power spectra

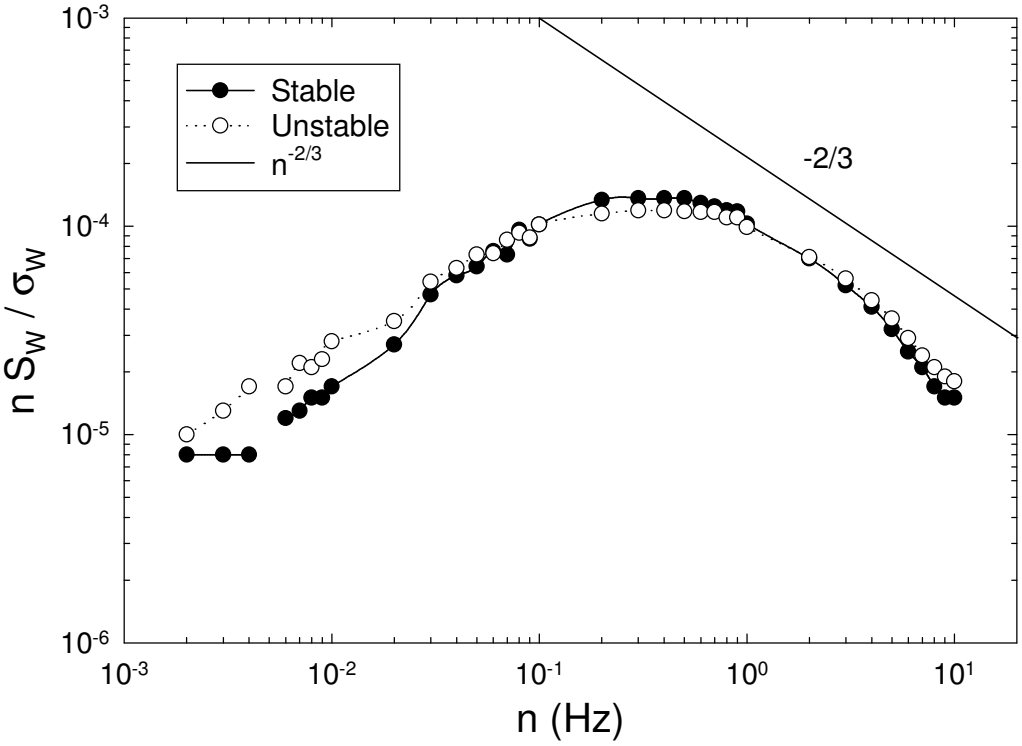

Figure 4. Stable ($-3 < \zeta < -2$) and unstable ($+2 < \zeta < +3$) natural frequency weighted vertical velocity power spectra (S_W) averaged over the duration of the GRAMINAE integrated experiment.

Figure 4 shows two power spectra of the vertical wind speed. These are averages of all W power spectra for each 15 minute logging period during the field campaign falling into the prescribed frequency ranges ("stable", $-3 < \zeta < -2$, – "unstable", $+2 < \zeta < +3$). The predominant features of interest here are the low frequency and inertial

sub-range gradients. In the low frequency (energy containing, – chapter 2) range, the power spectral density increases proportionally to n^{+1} as expected. This gradient in a frequency-weighted plot indicates a constant variance per frequency interval.

In the inertial subrange, the power spectrum is proportional to $n^{-2/3}$. This is as originally predicted by Kolmogorov (1941) and verified by numerous authors since, most notably in published analyses of the data from the 1968 AFCRL (Air Force Cambridge Research Laboratories) experiment in Kansas (Kaimal *et. al.*, 1972). Examination of the W power spectrum at all stabilities during all periods of the experiment shows similar agreement with the theoretical predictions.

The adherence of the spectra in figure 4 to the predicted shape provides some confidence that the vertical wind velocity has been correctly measured. Next, the power spectra of the aerosol concentration time series (S_N) are examined.

4.3.3 Aerosol concentration power spectra

The analysis of the *N* power spectrum presented here is designed to show the frequency response of the CPC. The inherent assumption is that pollutants should be *transported* in the same way as heat. That is, that the stability corrections (chapter 2) and the inertial sub-range of power and co-spectra should behave in the same way (note that there is no suggestion in the literature that the observed low frequency ranges of S_N and S_W should be similar). Although there are far fewer published spectral analyses of pollutant transport than of heat and momentum transport, and even fewer relating to aerosol transport, this assumption appears to generally work well except in circumstances where the measurement equipment introduces its own frequency dependent behaviour (damping, slow response).

As stated above, the inertial sub-range prediction for the power spectral density for heat and inert pollutant transport is the same as for vertical velocity; – S_N should decrease as $n^{-2/3}$. The spectrum is shown in figure 5, and looks significantly different to the plot of S_W in figure 4. Again, the spectrum is an average of all 15 minute

periods during the experiment, with the "stable" plot representing $-3 < \zeta < -2$ and the "unstable" plot $+2 < \zeta < +3$.

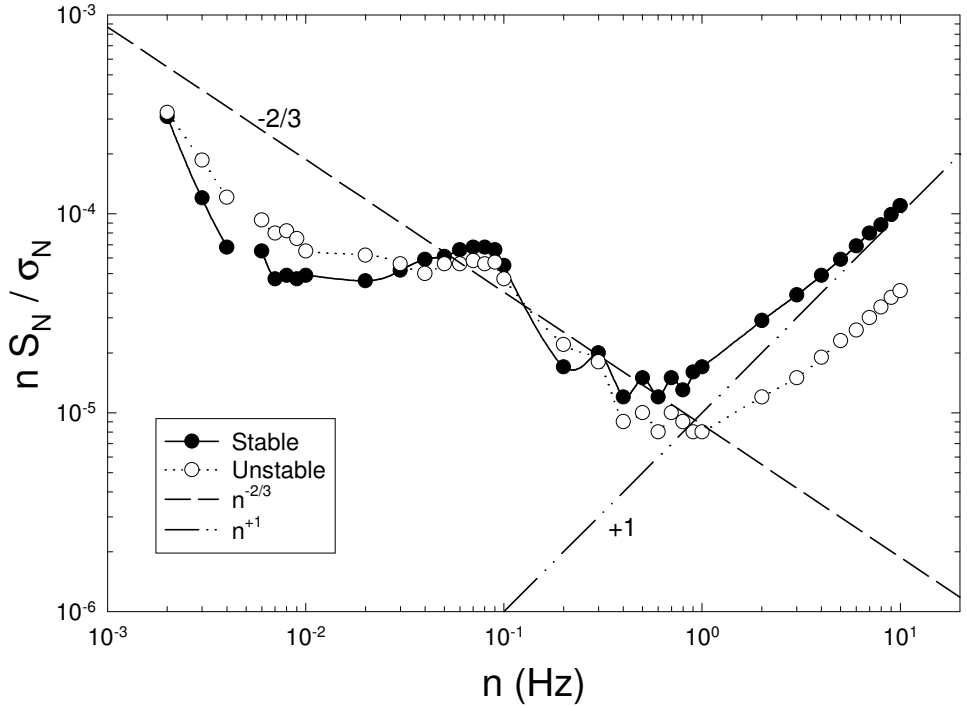

Figure 5. Stable ($-3 < \zeta < -2$) and unstable ($+2 < \zeta < +3$) natural frequency weighted aerosol concentration power spectra (S_N) averaged over the duration of the GRAMINAE integrated experiment.

There are two significant areas of difference between S_N and S_W. These are at the low frequency and high frequency extremes of the plot. In between these there is an observable inertial sub-range between 0.08 Hz and 1 Hz (periods of 12.5 to 1 second). At low frequency S_N increases with *reducing* frequency (*c.f.* figure 4) below around 0.007 Hz; this is equivalent to variations in aerosol concentration over a period of two to two and a half minutes (exactly 143 seconds). This is not observed in S_W because the vertical wind speed cannot vary significantly over such a long period due to the presence of the surface, except where gravity (or lee) waves are operating. There is no such constraint on the variability of aerosol concentration. Interpretation of such large-scale motions is left until the discussion of the WN co-spectrum (C_{WN}).

The second major difference between S_W and S_N is at higher frequencies. Beyond the inertial sub-range S_N increases as n^{+1}. As stated in chapter 2, this is indicative of white noise. In this frequency-weighted representation of the *N* power spectrum, a gradient

of n^{+1} means constant variance per unit frequency interval, – *i.e.* the CPC appears not to be resolving changes in aerosol concentration at this rate.

The above considerations mean that in this experimental set-up, the CPC flux system does not, on average, resolve changes in aerosol concentration faster than around 1 Hz. It is important to note however, that this does not necessarily represent an inherent upper limit of 1 Hz to the frequency response of the CPC flux system, but rather that in the conditions encountered during the GRAMINAE integrated experiment concentration fluctuations were not accurately observed above this frequency. During certain periods the onset of white noise was delayed until n = 4 Hz, giving rise to the possibility that the effect is due in part to low mean concentrations, and that large variations in aerosol concentration can be resolved up to at least 3 – 4 Hz. Investigation of individual aerosol spectra may go some way towards confirming this, but the scatter inherent in such plots makes this an uncertain exercise. The effect of the evident frequency dependent reduction in CPC response on the measured aerosol fluxes will be discussed in the next section.

4.3.4 Aerosol flux co-spectrum

The frequency-weighted co-spectrum of W and N (C_{WN}) is shown in figure 6. The inertial sub-range prediction of Kolmogorov (1941) and of Wyngaard and Coté (1972) for frequency weighted (normalised) co-spectral density is of a decrease in proportion to $n^{-4/3}$ (the equations are presented in chapter 2). This is observed in figure 6 between 0.1 Hz < n < ~3 Hz. The highest values lie at the low frequency end of the plot, however, the gradient in this area is not as steep as in S_N. This shows that the long period variations in N are not correlated with the vertical wind speed and do not contribute significantly to the calculated flux.

The scatter evident in both co-spectra is typical of aerosol data. It is caused by the counting statistical problems outlined above and in chapter 2. It is unclear whether the data above 3 – 4 Hz should be fitted by n^{+1} or whether the values are approximately constant. What is clear is that the predicted $n^{-4/3}$ decrease is not present. This means that the white noise demonstrated in figure 5 is uncorrelated with vertical velocity and

that the portion of the flux transported at high frequencies is not properly resolved by the CPC flux system under the prevailing field conditions.

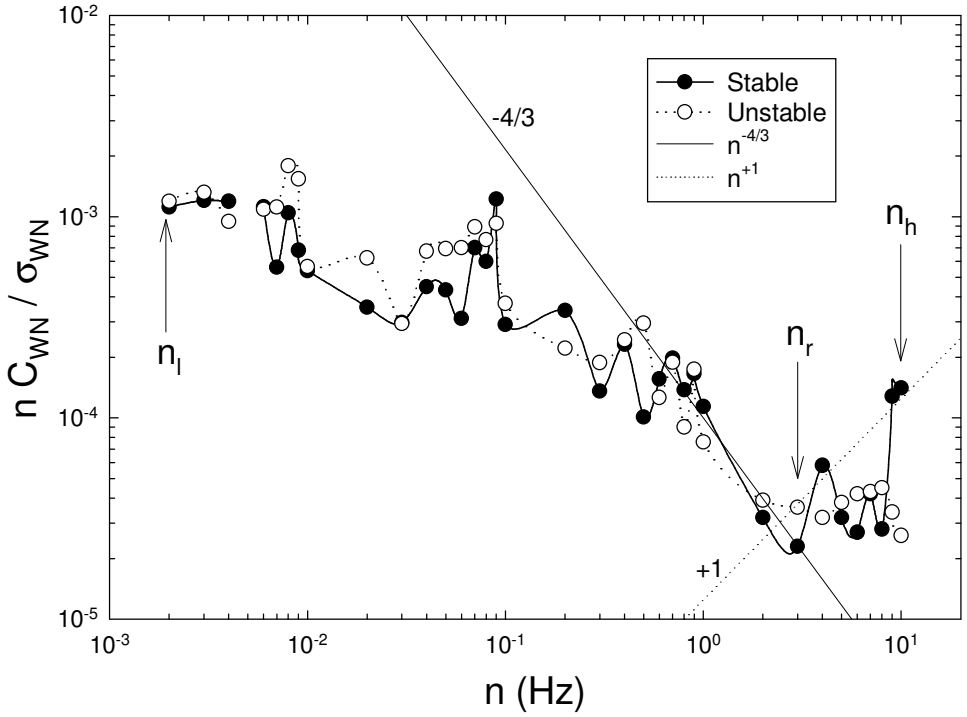

Figure 6. Stable (-0.5 < ζ < -0.3) and unstable (+0.5 < ζ < +0.3) natural frequency weighted aerosol concentration / vertical velocity co-spectra (C_{WN}) averaged over the

The effect of the high frequency noise in C_{WN} on the measured flux is a question of interest as it reflects on the reliability of the data from the UMIST CPC system. Several attempts have been made to model and thus quantify the influence of inadequate high frequency response on pollutant flux measurements. The best known such work is that of Eugster and Senn (1995). They examined data from a "fast" response NO_2 analyser (Unisearch Scintrex LMA-3), and interpreted the high frequency signal losses by analogy with inductance in an electronic circuit. A general method was presented for correcting data for these "inductive" losses. They found losses in the total flux of between 10% and 30 %. However, their reasoning predicted an increased gradient in the inertial sub-ranges of the scalar sensor's power spectrum and the co-spectrum (respectively $n^{-5/3}$ and $n^{-8/3}$ in frequency weighted plots). This behaviour was not observed in the current data set, making the application of the Eugster and Senn (1995) corrections to this data a questionable exercise. In any case,

as will be demonstrated later, such attention to detail is not required to validate the flux measurements.

There are three frequencies indicated in figure 6; – these are n_l, n_r and n_h. The first, n_l is the lowest frequency in the transform (equating to a period of around eight minutes). The second, n_r is the frequency at which the inertial sub-range behaviour breaks down and noise begins. n_h is the highest frequency in the transform (the system was logged at 20 Hz, so this, the Nyquist frequency, is 10 Hz). Now, apart from those properties noted in chapter 2, the co-spectrum has the property that:

$$f_N = \int_{n_l}^{n_h} C_{WN}\, dn \tag{4.2}$$

where f_N is the aerosol flux, n is frequency and C_{WN} is the W N co-spectrum. An approximate integration of the average of the two curves shown as figure 6 in the two regions bounded by $n_l - n_r$ and $n_r - n_h$ shows that the properly resolved part of the spectrum between n_l and n_r contributes 97.74% of the total measured flux. Note that the reason this does not appear to be the case on first inspection is that figure 6 is frequency weighted and the high frequency values are artificially increased. In effect

$$f_N = \int_{n_l}^{n_r} C_{WN}\, dn \qquad >> \qquad f_N = \int_{n_r}^{n_h} C_{WN}\, dn \tag{4.3}$$

The point of this analysis is to show that while it may be possible to develop a model to correct the shape of C_{WN} at high frequencies, it would not significantly alter the values of fluxes reported. This being the case, the measured fluxes were left unaltered, and in the interest of simplicity, spectral correction models have not been used. Having verified the validity of the fine mode aerosol flux measurements in general, the results are presented in the following sections.

4.3.5 Interpretation of Diameter range of Aerosol Measurements

The first question to be addressed in interpreting the total aerosol number fluxes from the CPC measurement system is the diameter of aerosol to which the data are applicable. Since the measured fluxes are representative of an extremely broad diameter range (0.011 μm < D_p < 3 μm), it is important to determine which size range the measurements actually represent. In chapter 5 it is shown that for ambient urban aerosol concentrations, the CPC size range, number weighted, is only representative of the diameter interval 11 nm < D_p < 100 nm. However, rural size distributions are, in general, not the same as urban distributions, so this need not be the case here.

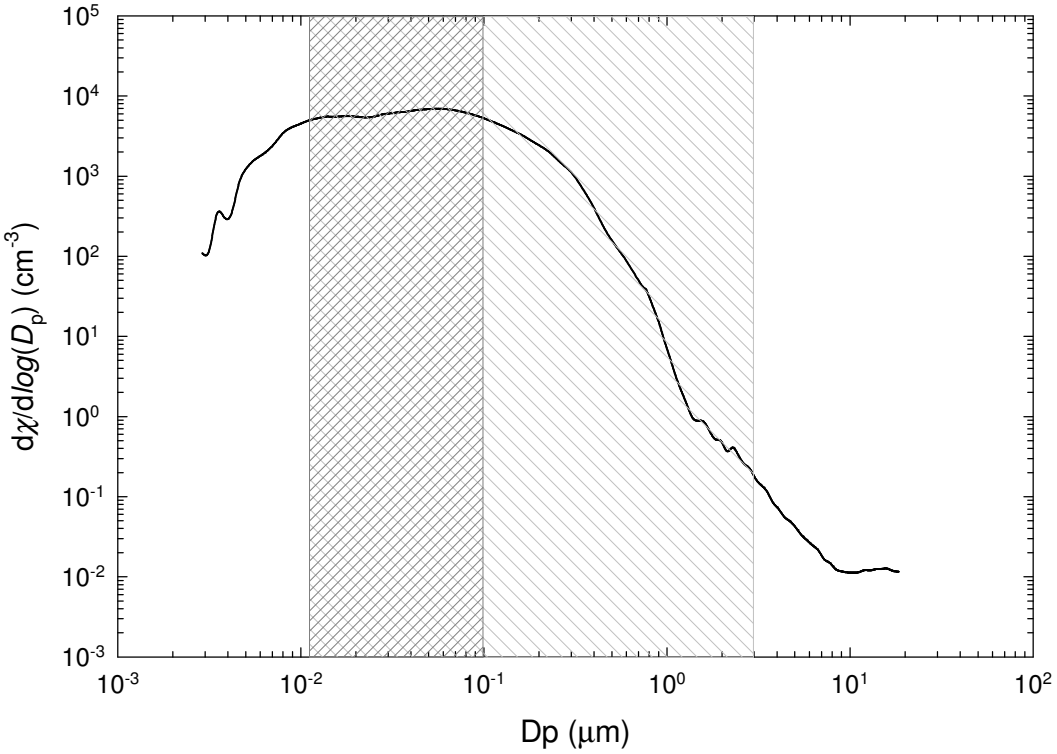

Figure 7. Average combined DMPS and APS spectrum over the majority of the GRAMINAE integrated experiment. Periods of mechanical works (*i.e.* cutting, lifting, turning) have been excluded as far as possible.

The first task is to examine the ambient aerosol distributions during the first two significant analysis periods (long and short canopies) and determine the diameter range whose dynamics determine the observed fluxes. Data from the UMIST DMPS

(Williams, 2000) Differential Mobility Particle Sizer is used in this section to calculate exactly which are the "active" diameter ranges.

Figure 7 shows the average aerosol size distribution from 2.8 nm to 19 μm during the integrated experiment. The extension above the DMPS diameter range is achieved by concatenating the APS concentration distribution with the DMPS data. The heavily shaded area covers the range 11 nm < D_p < 100 nm, while the lightly hatched region indicates the diameter range of the CPC flux measurement system. The aerosol concentration in the 11 nm < D_p < 100 nm region is 84% of the concentration in the range 2.8 nm < D_p < 19 μm, meaning that although the dominance of the sub 100 nm range is not quite as clear as in the urban environment (chapter 6), it is certainly reasonable to assume that the results obtained are representative of the dynamics of aerosol in the range 11 nm < D_p < 100 nm (denoted by D_3 in chapter 6). Obviously, the comparatively low concentration observed at this rural site at all sizes means that this interpretation of the CPC fluxes may not be strictly valid at all times due to the inevitable variability in the concentration distribution, but it does give a better indication of the size range observed than the total CPC response range of 11 nm < D_p < 3 μm.

4.4 Fine Mode Results

Fluxes of fine mode aerosol have been measured recently above boreal forest (Buzorius *et.al.*, 1998), heathland (Nemitz *et. al.*, 2002 a) and Edinburgh city centre (chapter 6, Dorsey *et. al.*, 2002). No measurements had been made above grass canopies prior to the GRAMINAE integrated experiment. Deposition velocities for both long and short canopies will be presented here, together with a discussion of the dynamics of the aerosol deposition process.

Table 4 contains a summary of the surface deposition velocities, v_{ds}, and major parameters used to describe the canopy structure. The deposition velocities are extremely low, compared to the values calculated from the ASASP-X / Gill 1012 R data.

	U Ms^{-1}	RH %	T_a ^oC	χ cm^{-3}	σ_T ^oC	σ_N cm^{-3}	λE Wm^{-2}	H Wm^{-2}
Long canopy	2.16	72.60	13.36	7936.58	0.3193	864.91	64.67	-5.30
Short Canopy	2.23	65.68	18.60	8143.53	0.4845	633.44	55.85	49.51
Post fertilisation	2.61	73.04	17.64	9309.16	0.3797	1073.55	77.80	30.23
All Periods	2.41	71.40	15.94	8532.07	0.3978	1693.10	70.30	25.38
	σ_U/u_* #	σ_V/u_* #	σ_W/u_* #	f_χ $cm^{-2}s^{-1}$	v_{ds} mms^{-1}	u_* ms^{-1}	u_*/U #	z_0 m
Long canopy	3.08	2.87	1.26	-229.11	0.3650	0.25	0.12	0.07
Short Canopy	4.10	3.80	1.41	-25.95	0.1373	0.20	0.10	0.02
Post fertilisation	3.65	3.57	1.35	383.31	-0.5213*	0.23	0.09	0.04
All Periods	3.55	3.42	1.33	367.48	-0.3292	0.23	0.10	0.05

Table 4. Summary of fine mode (0.011 μm < D_p < 3.0 μm) aerosol deposition data. v_{ds} = surface deposition velocity, χ = concentration, z_0 = roughness length, h_c = canopy height, σ = standard error (a measure of the error of the calculated quantity). * The value of v_d for the post fertlisation period is the unmodified measured value (including r_a).

4.5 Aerosol deposition model

The reason for these low fine mode deposition velocities to both long and short canopies compared to those observed in the accumulation mode is shown in figure 8.

Figure 8 shows the Zhang *et. al.* (2001) implementation of the Slinn and Slinn (1980), Slinn (1982) aerosol deposition framework. The total deposition velocity can be calculated according to equations 2.30 and 2.33, giving

$$v_d = v_g + 1/(r_a + r_s) \tag{4.4}$$

with r_a = aerodynamic resistance (2.34) and r_s is the surface resistance to deposition. In fact, the definition of r_a in the model of surface resistance calculates the wind speed from u_* and z_0, but agreement with measurements is excellent (in this case well within 5%). r_s is calculated according to:

$$r_s = 1/(\varepsilon_0 u_* (E_b + E_{im} + E_{in}) R_s) \tag{4.5}$$

where ε_0 is an empirical constant (= 3) and E_b, E_{im} and E_{in} are the efficiencies of Brownian diffusion, impaction and interception in the canopy respectively. R_s represents the "sticking efficiency", – the probability of particles rebounding from the canopy rather than being deposited. E_{im}, E_{in} and v_g all increase with increasing D_p, resulting in larger deposition velocities for large particles. E_b (and hence Brownian diffusion) however, is very high for fine mode particles. The sticking efficiency also reduces markedly for large particles. This results in the shape of figure 8.

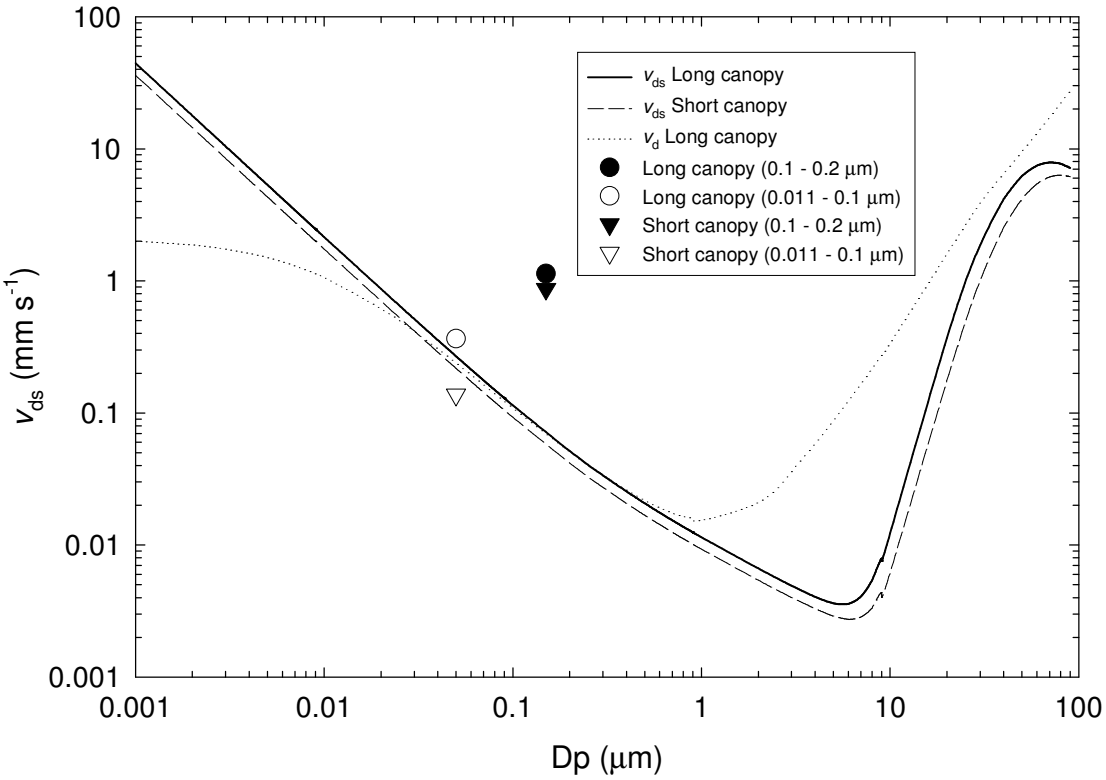

Figure 8. Zhang *et. al.* (2001) implementation of the Slinn (1980, 1982) framework for aerosol deposition velocity. Here $v_d = v_g + 1/(R_a + R_s)$ except where the turbulent deposition velocity ($v_d - v_g$) is shown. Accumulation mode (Gallagher *et. al.*, 2002) and fine mode (CPC flux system) deposition velocities are included.

All quantities in equation 4.5 were defined as suggested by Zhang *et. al.* (2001) except E_{im}, which was calculated using the formulation of Giorgi (1986) for vegetated surfaces. For ease of repeatability, the full model formulation is presented in Appendix A, including all of the required definitions not supplied by Zhang *et.al.* (2001).

The observed surface deposition velocities fit reasonably well with the model predictions in the fine mode. The points representing deposition velocity are shown in the middle of the measured size ranges (i.e. 0.15 μm for the ASASP-X and ~ 50 nm for the CPC system, but note the uncertainty mentioned above in the exact size of the fine mode range). The trace of v_d (total) is intended to show that at the size ranges considered here, gravitational settling is unimportant, becoming a factor only at $D_p >$ 1 μm. Also, the aerodynamic resistance appears to make little difference to the total deposition velocity for this range of particle diameters. This is due to the fact that the predicted surface deposition velocities are so low that adding r_a to r_s makes little difference to the total.

There is a large discrepancy between the Zhang *et. al.* (2001) model and the accumulation mode measurements. Other aerosol deposition models give different predictions in the accumulation mode (e.g. Slinn and Slinn, 1980; Slinn, 1982) and these models tend to predict higher deposition velocities for accumulation mode particles than the one presented here. As stated in the section on the accumulation mode deposition measurements, these measurements are entirely consistent with other experimental determinations. It appears, therefore, that the discrepancy is due to the model in this size range, rather than the measurements.

Ruijgrok (1995) notes that the accumulation mode is one of the largest areas of uncertainty in deposition models. Gallagher *et. al.* (1997) find, in their review of aerosol deposition measurements, that deposition velocities are significantly under-estimated by the available models in this size range, especially over rough surfaces. This is an outstanding problem, which will only be addressed by further measurements such as those presented here and model development in the light of these results.

4.6 Fine mode deposition velocity trends

There have been few studies published on fine mode deposition velocities measured by eddy covariance. However, there is a friction velocity dependence (*c.f.* figure 3, for

roughness length), as suggested by equation 4.5. Figure 9 is taken from Nemitz *et. al.* (2002 a), and compares deposition velocities from several studies.

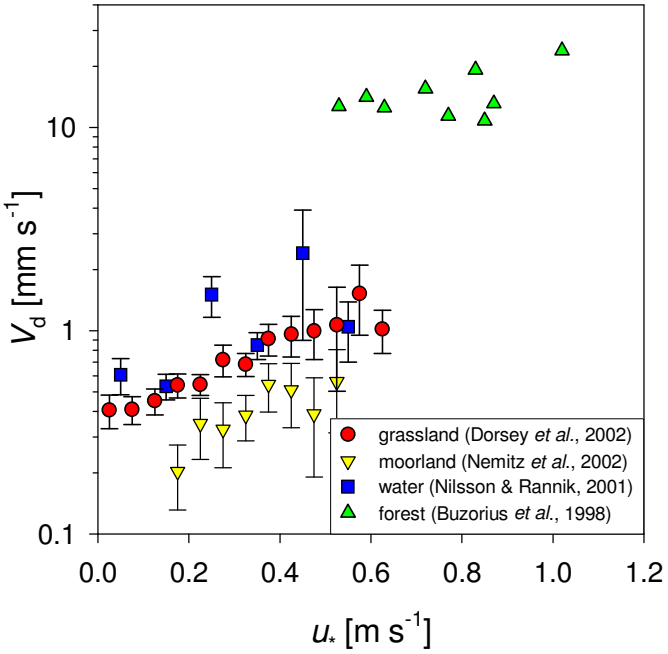

Figure 9. Friction velocity dependence of deposition velocity. Taken from Nemitz *et. al.* (2002)

4.7 Summary of results

Analysis of the data gathered during the GRAMINAE integrated experiment (22nd May – 15th June 2000) has shown that accumulation mode (0.1 µm < D_p < 0.2 µm) aerosol deposition velocities were 1.13 mm s^{-1} and 0.87 mm s^{-1} to long and short grass canopies respectively. The corresponding fine mode deposition velocities were 0.2747 mm s^{-1} and 0.0658 mm s^{-1}, where the long canopy height was 0.65 m – 1.0 m with a roughness length of 0.063 m and the short canopy height was 0.07 m – 0.14 m with a roughness length of 0.022 m.

The measurements of fine mode aerosol fluxes were examined in detail to ensure that the measurement technique was valid for this experiment. The size range represented by these measurements was shown to be from 11 nm up to around 100 nm (the D_3 range).

The accumulation mode deposition velocity results fit well the roughness length dependence suggested by Gallagher *et. al.* (2002) in their reanalysis of deposition data from other experiments. A "Slinn type" aerosol deposition model has been compared to these results, and agreement with observation was found to be poor in the accumulation mode. The uncertainty in the current knowledge of deposition processes, and the variability in the predictions of this type of model have been noted.

Fine mode deposition velocities were found to be significantly lower than the values for the accumulation mode. Fine mode flux measurements are a recent development, and there are not enough data over a sufficient range of canopy types (roughness lengths) in the literature to show any trend in the roughness length dependence of deposition velocity. The measurements do, however, fit well with the results of the deposition model discussed above and with the trend with friction velocity observed in other, similar studies.